Wang et al. Nanoscale Research Letters (2016) 11:342
DOI 10.1186/s11671-016-1556-9

Nanoscale Research Letters

NANO REVIEW Open Access

Overview of Probe-based Storage Technologies

Lei Wang*, Ci Hui Yang, Jing Wen, Si Di Gong and Yuan Xiu Peng

Abstract

The current world is in the age of big data where the total amount of global digital data is growing up at an incredible rate. This indeed necessitates a drastic enhancement on the capacity of conventional data storage devices that are, however, suffering from their respective physical drawbacks. Under this circumstance, it is essential to aggressively explore and develop alternative promising mass storage devices, leading to the presence of probe-based storage devices. In this paper, the physical principles and the current status of several different probe storage devices, including thermo-mechanical probe memory, magnetic probe memory, ferroelectric probe memory, and phase-change probe memory, are reviewed in details, as well as their respective merits and weakness. This paper provides an overview of the emerging probe memories potentially for next generation storage device so as to motivate the exploration of more innovative technologies to push forward the development of the probe storage devices.

Keywords: Probe, Density, Storage medium, Memory, Data

Review

Introduction

Today, the prosperity of social networks such as Youtube, Twitter, and Facebook, in conjunction with the digitalization of the daily service of worldwide citizens, has triggered a radical increase on the total amount of global digital data. According to IDC's report, the amount of digital data has already surpassed 4.4 ZettaBytes (ZB) in 2013, and is predicted to reach 44 ZettaBytes in 2020 [1]. Under this situation, the capacities of various data storage devices where the digital data can be recorded and replayed are conversely limited in TeraBytes (TB) regime, lagging far behind the phenomenal growth of the digital data. The conventional mass storage devices can be categorized into hard disk, optical disc, and flash memory. Today, the hard disk drive (HDD) is undoubtedly the most famous mainstream storage device mainly due to its high capacity, fast data rate, and low cost. Nevertheless, in order to satisfy the current storage demand, the magnetic grain inside the HDD needs to be further shrunk so as to enhance the resulting density. However, the reduction on the volume of the magnetic grain would deteriorate the thermal stability of the magnetic written bits whose magnetization may be reversed without magnetic field due to the thermal fluctuation. This is well-known as superparamagnetic limit [2, 3]. The evolution of the optical disc has experienced three generations ranging from compact disc (CD) to Blu-ray disc. The major hurdle to prevent optical disc from booming its capacity results from the fact that the diameter of the laser spot focused on the optical disc is approximately proportional to the wavelength of the laser beam and inversely proportional to the numerical aperture (NA) of the objective lens [4, 5]. In this case, the storage capacity of the optical disc can seemingly be enhanced by either reducing the beam wavelength or increasing the NA. However, as there is no breakthrough progress recently made in the technologies of solid state laser and objective lens, the shortest wavelength and the largest NA to date are still limited to 405 and 0.85 nm for optical recording [6], which is usually referred to optical diffraction. Flash memory, represented by universal serial bus (USB) drive and iPhone series products, has recently received numerous attentions because of its high capacity, short data access time, non-volatility, portability, and low expense, which is expected to replace HDD in the near

* Correspondence: LeiWang@nchu.edu.cn
School of Information Engineering, Nanchang HangKong University, Nanchang 330063, Peoples' Republic China

future. The capacity improvement of the flash memory strongly depends on the downscale of the flash cell size. In this case, further scaling down the cell size would result in a decrease on the thickness of the tunnel oxide layer usually sandwiched between the floating gate and wafer. A tunnel oxide layer with a very thin thickness is unable to prevent electrons from escaping from the floating gate, thus causing the loss of data, which is known as scaling limit [7, 8]. Consequently, as HDD, optical disc, and flash memory are suffering from superparamagnetic limit, diffraction limit, and scaling limit, it is timely to explore more innovative mass storage devices with higher storage capacity, faster data rate, lower energy consumption, and longer data retention time than conventional counterparts, giving rise to the advent of probe-based storage devices.

A probe-based storage device can be defined as a storage memory that utilizes nanoscale probe to record and read bits in the storage medium. Prior to the probe-based storage device, nanoscale probe has been widely used for scanning probe microscope (SPM) applications to map out the tomography image of the sample [9]. To achieve this, nanoscale probe usually makes use of a cantilever with a very sharp tip integrated on its end to perform the raster scanning in which tip is brought closely to or in contact with sample. During the scanning, the tip can be deflected up or down due to the variation of the atomic force between tip apex and sample surface, and tomography image of sample surface can therefore be constructed by measuring the position of the tip, as schematically shown in Fig. 1. For probe-based storage device, an external excitation that is initially applied to the nanoscale probe can be employed to change the physical properties of the storage medium when in contact with the probe tip during the scanning, and thereby the region subjected to the external excitation exhibits different physical properties from the region without suffering from the excitation. As a result, these two regions with different characteristics can be regarded as the binary bits "1" and "0", respectively, to realize the storage function. The principle of the probe-based storage device is illustrated in Fig. 2. According to the descriptions above, the size of the recorded bit is primarily determined by the size of the tip apex used for recording process, implying a fact that the implementation of tip apex on the order of nanometers would allow for an areal density over multi Terabit per square inch ($Tbit/in^2$). In addition, the small size of recorded bit can lead to an aggressive reduction on the required energy consumption. Thanks to these merits, worldwide researchers have been dedicated to exploring probe-based storage technologies using various storage materials and system architectures, and this gives rise to an emergence of a variety of innovative probe memories such as thermo-mechanical probe memory, magnetic probe memory, ferroelectric probe memory, and phase-change probe memory. In this case, it is essential to have a thorough review on the physical principles and current status of various probe-based storage devices to help scientists to understand the inherent physics of these devices. However, such review articles are rarely found according to Web of Science by the time of writing and the latest review article about probe storage technologies has been dated back to 2011 [10]. As a result, a comprehensive review concerning probe-based storage devices is urgently required so as to reveal the physical mechanisms of these devices, and thus to ignite the research enthusiasm to further mitigate their respective storage performances.

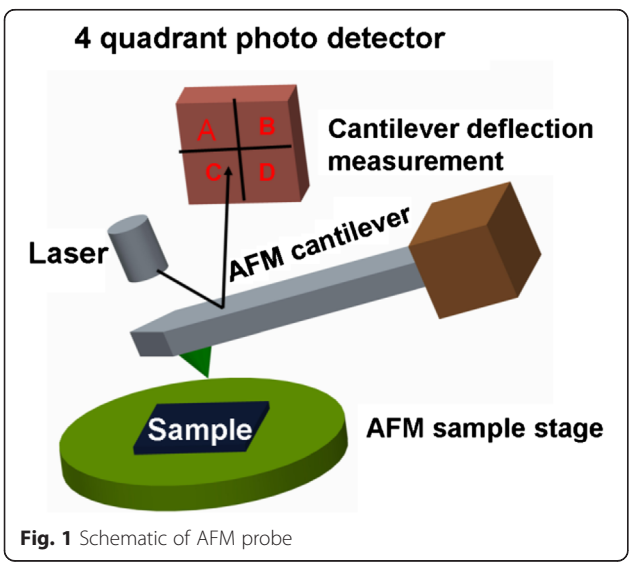

Fig. 1 Schematic of AFM probe

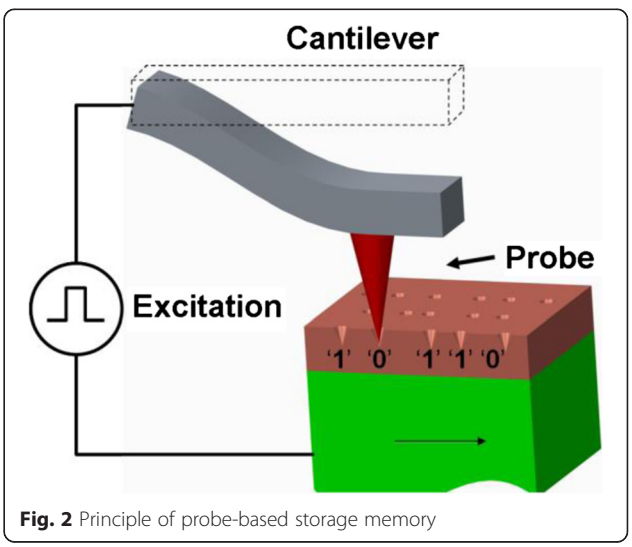

Fig. 2 Principle of probe-based storage memory

Thermo-Mechanical Probe Memory

The principle of thermo-mechanical probe memory is to pull a heated tip into the polymer medium to generate topographic change that can be denoted as binary digit "1" on medium surface [11]. The driving force behind the development of thermo-mechanical probe memory can be ascribed to the presence of IBM's Millipede system that consists of an array of SPM tips with a moving storage medium underneath [11], as shown in Fig. 3. A localized heater, usually made of low-doped resistive silicon is integrated at the tip base, acted as heating element. During the writing process, an electrostatic force is applied to the cantilever to push the tip that is heated around polymer's glass transition temperature (400 °C) into the polymer medium to soften it. The heated polymer medium would melt and allow tip to penetrate into it, thus generating an indentation on medium surface. This indentation and surrounding continuous flat surface can be used to represent "1" and "0", respectively. The erasing process can be achieved by removing the applied force to pull the tip up back from the indentation. This would result in a surface tension to flatten the previously written indentation [12]. During the readout process, a read resistor whose resistance strongly depends on the temperature is integrated in one of the side-arms of the three-legged cantilever design, which is heated to around 300 °C. When tip falls into an indentation, the distance between tip and substrate is reduced, thereby accelerating heat leaking through the substrate. In this case, the temperature of the read resistor is changed due to the cooling process, and this would change the resistance of the read sensor, which can be detected as readout signals. The writing, readout, and erasing modes of thermo-mechanical probe memory are schematically shown in Fig. 4.

The ability to simultaneously record and read bits using tip arrays obviously endows thermo-mechanical probe memory with some advantageous traits such as ultra-high recording density and high data/write speed when in comparison with conventional data storage devices [13–16]. In addition, the resulting density can be further boomed by reducing the bit pitch that is determined by the rim size of the written bit [17]. It has been found that either using a tip with small contact radius or reducing the indentation depth can effectively compact the rim size, and therefore allow for higher recording density. These exciting findings and the inherent advantages of device itself have recently led to some remarkable technological advances on thermo-mechanical probe memory. In perspective of the storage medium, a Diels-Adler (DA) polymer that has a highly cross-linked, high-molecular weight at low temperature was proposed [18]. This polymer has a high wear resistance with good thermal stability below the transition temperature, whereas it turns out to be easily deformable and gentle on the tip above the transition temperature. The feasibility of using DA polymer to achieve 1 Tb/in^2 has been demonstrated [18]. In addition to DA polymer, a polyaryletherketone (PAEK) polymer that unites phenylethynyl groups in the backbone with diresorcinol units in the backbone for control of the glass-transition temperature was considered as another promising storage medium for thermo-mechanical probe memory due to its low glass-transition temperature less than 160 °C in the cross-linked state and superb thermal stability up to 450 °C [17]. These exceptional characteristics would give rise to a writing of indentation on a microsecond time scale as well as an effective minimization of thermal degradation for indentation with a hot tip. The capability of using a PAEK polymer templated on a cleaved mica surface to provide an areal density of 4 Tb/in^2, the endurance of 108 write cycles, and data retention time of 10 years at 85 °C has been demonstrated [19–21], as illustrated in Fig. 5. The possibility of achieving 9 Tb/in^2 based on the PAEK polymer was also theoretically predicted [22]. Another prospective material for thermo-mechanical recording as an alternative to polymer is NiTi shape-memory alloys (SMAs) [23]. NiTi is more immune to the normal environment effects at the shape-memory effect's normal operation temperature than the poly (methyl methacrylate) (PMMA) polymer that is apt to charring at the temperatures around

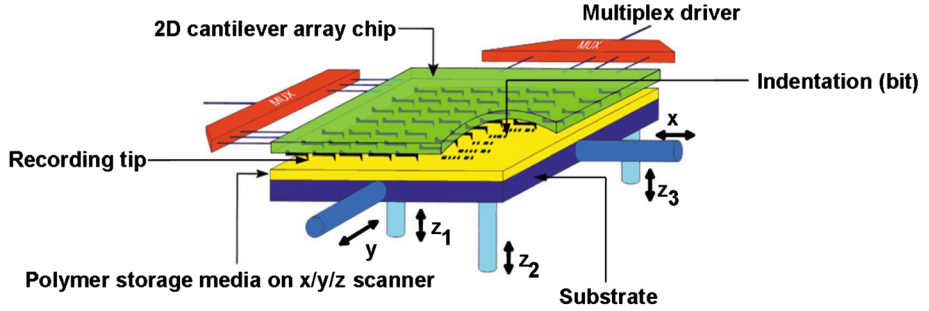

Fig. 3 Millipede system. Reprinted with permission from [11]

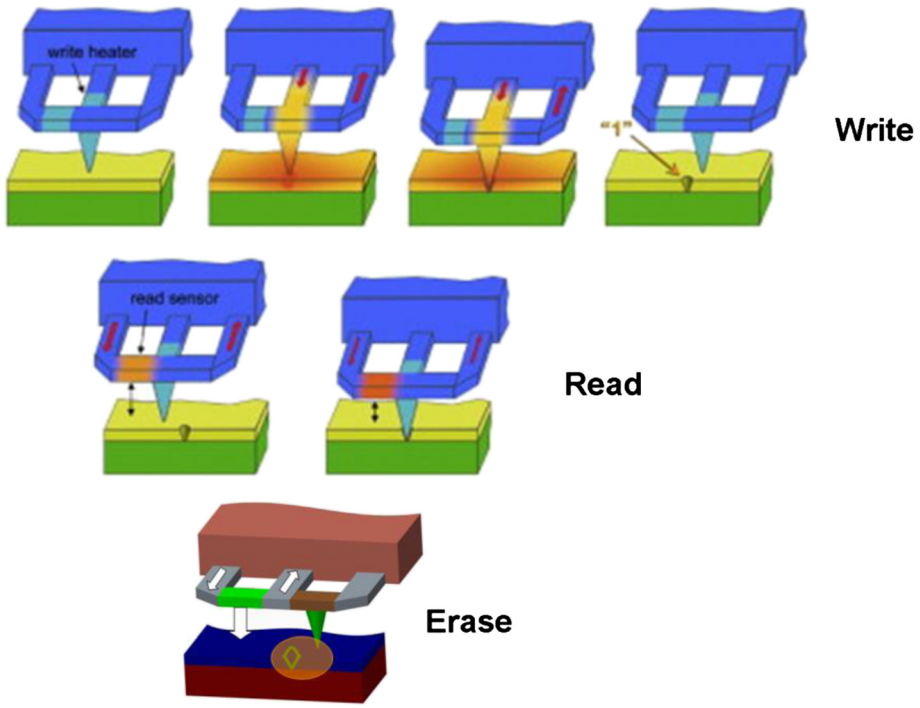

Fig. 4 Millipede memory when operated in write mode, read mode, and erase mode. Reprinted with permission from [13]

350 °C. Besides, the low operating temperature and high thermal conductivity of SMAs allows the device using SMAs to have a less energy consumption for writing and more rapid erasing operation than that with PMMA polymer. The practicality of using SMAs as the storage medium for thermo-mechanical probe storage to achieve 0.5 Tbit/in^2 has already been proven [23].

As thousands of cantilevers scan repeatedly back and forth across the medium surface, the tip and sample wear become more evident than other storage devices, thus exacerbating the lifetime of the thermo-mechanical

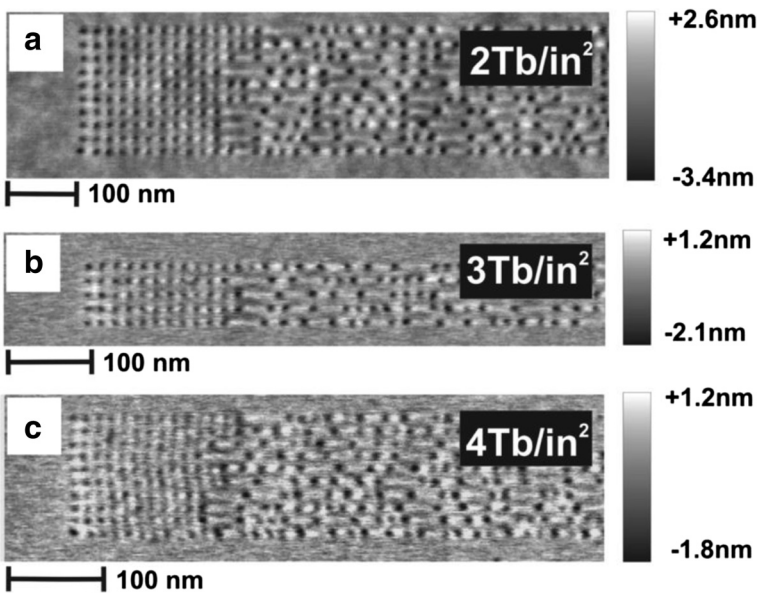

Fig. 5 Topographic images of random data patterns used in the recording tests showing (**a**) 2 Tbit/in^2 on a normal spin coated samples, and (**b**) 3 Tbit/in^2, and (**c**) 4 Tbit/in^2 on an ultraflat templated sample. Reprinted with permission from [17]

probe device as well as the resulting density. In order to suppress the wear from media's point of view, one possible approach is to introduce a photo-resistant layer between the silicon substrate and the PMMA polymer [12]. From the perspective of tip, tip wear can be aggressively mitigated by coating the tip with some hard materials. Recently, a moulded DLC tip designed based on atom by atom attrition mechanism was reported to give approximately four orders of magnitude improvement on wear compared to the carbon nanotube tip [24]. Such an improvement can be further enhanced by the use of SiC tip [25]. Another possibility to alleviate the tip wear is to actuate the tip with a periodic force at frequencies at or above the natural resonant frequency of the cantilever [26, 27]. In practice, it is preferable to operate AFM at intermittent-contact mode that can effectively reduce tip wear. However, the intermittent-contact mode that usually requires high cantilever stiffness is usually contradictory with the feeble cantilever used in thermomechanical storage to allow easy electrostatic actuation [28]. This can be solved by either utilizing amplitude modulation of the cantilever through electrostatic actuation [26] or slightly modulating the force on the tip-sample contact [28], allowing for an areal density of 1 Tb/in^2 attained even after a sliding distance of 140 m.

Magnetic Probe Memory

Magnetic probe memory exhibits an analogous recording/readout mechanism to the conventional HDD. A probe tip from magnetic force microscope (MFM) scans over the surface of the magnetic medium whose magnetization can be reversed by the magnetic field emanated from the magnetic tip, to accomplish the recording operation, as illustrated in Fig. 6. During readout mode, the MFM tip is brought in close to the previously written magnetic dots and thus deflected up and down due to the magnetic force existing between the tip and magnetic dot. Such a variation of the position of MFM tip can be detected as the readout signal. It is well-known from the Neel-Arrhenius relation that the ratio of the product of the crystalline anisotropy and the volume of the bit to the product of the Boltzmann constant and the absolute temperature should be greater than 50 so as to maintain the thermal stability of the magnetic dots [29]. In this case, the reduction on the bit volume for higher density would require a larger crystalline anisotropy, thereby requiring a much higher writing field from magnetic tip. Nevertheless, due to the low field emanated from the magnetic tip, the crystalline anisotropy of the storage medium for magnetic probe memory needs to remain low to ensure the successful magnetization reversal while at the expense of the resulting recording density. For this reason, the magnetic probe memory has initially shown a relatively low recording density down to 200 Gb/in^2, resulting from a vacuum MFM on Co/Pt multi-layered dots with perpendicular anisotropy [30, 31]. Fortunately, several methods to strongly enhance the writing field of MFM probes have been proposed recently, one of which is to applying an external field on a small coil mounted below the magnetic medium [32–38]. As can be seen from Fig. 7, the magnetization of the recorded film can be reversed by the superimposition of the writing field directly from MFM tip and the external field from the coil, leading to a density possibly up to 1.2 Tb/in^2 by mean of a 30 nm tip radius [37, 38]. An alternative to achieve the magnetization reversal in the absence of the external field is to locally heat the medium using a tunneling current from scanning tunneling microscope (STM) probe to lower its crystalline anisotropy [39–43], as illustrated in Fig. 8. Thanks to this, the magnetization of the heated region can be switched by the demagnetization field of the surrounding film. This technique results in a variety of bit size on Co/Pt multi layers ranging from 800 to 170 nm probably due to the variations on medium itself and tip radius [44–48]. However, if the writing is performed using STM tip, the subsequent readout of the written bits can only be read by spin-polarized tunneling. In this case, MFM tip that is operated in field-emission mode is implemented instead of STM, by which a minimum bit size with 80 nm is secured with the assist of a pulse background field [32]. In addition to the methods above, such as heat-assisted

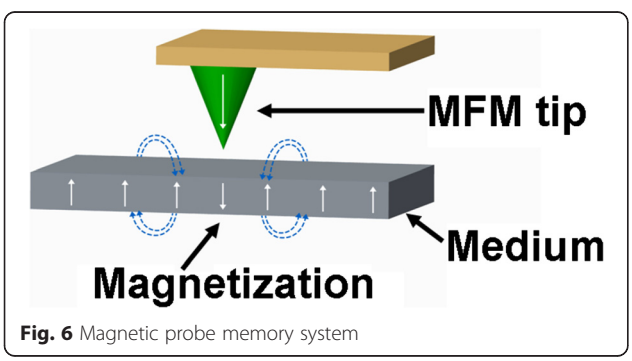

Fig. 6 Magnetic probe memory system

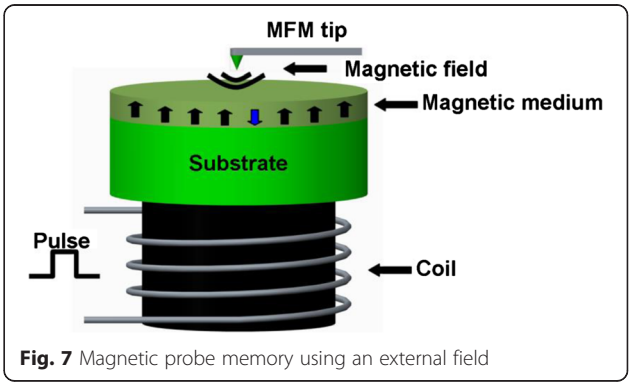

Fig. 7 Magnetic probe memory using an external field

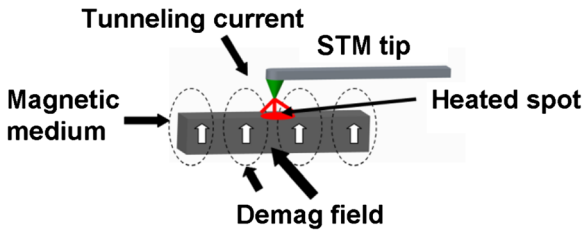

Fig. 8 Magnetic probe memory using STM

magnetic probe recording technology can be realized by an incorporation of a heated AFM tip with a Co/Pt multilayer patterned medium prepared by sputtering on pillars of 90 nm diameter [49], whereas the readout manner for this technique remain unreported. Such a nano-indentation technique was recently applied to a ferromagnetic shape memory alloy (FSMA) to achieve four magnetic-based memory states using MFM probe due to magnetic field or stress-induced twin rearrangement along two crystal orientations [50].

In terms of readout process, a short tip-sample distance on the order of 10 nm or less is required in order to obtain a readout image with high resolution. However, for MFM tip operating within such a small distance, non-magnetic tip-sample interactions play a more important role and would introduce unwanted topographic interference. This drawback can be overcome by integrating a magneto-resistive sensor on the magnetic tip [51–55]. A cantilever integrated with a spin-valve sensor was recently reported, and leads to a resolution around 1 μm, which is somewhat inadequate for probe-based storage [56]. However, it is possible to incorporate the magnetic field sensor used for modern HDDs that can readily give a resolution below 20 nm with the magnetic probe memory. In addition to this, another novel approach making use of dual tips for both topography and magnetic field imaging has been recently proposed [57]. According to this method, a cantilever is cut in half using the focused ion beam technique, whereby two different tips, one magnetized tip and one non-magnetized tip, are implemented to tackle the topography imaging and magnetic imaging, respectively. This dual-tip technique can radically suppress the perturbations of the magnetic tip as compared to the standard MFM methods.

Ferroelectric Probe Memory

The storage medium of ferroelectric probe memory is ferroelectric material showing a non-linear relationship between the applied electric field and the store charges. As illustrated in Fig. 9, applying an external electric field to the ferroelectric material can align its dipole with the field direction due to the small shifts in the position of atoms associated with shifts in the distributions of

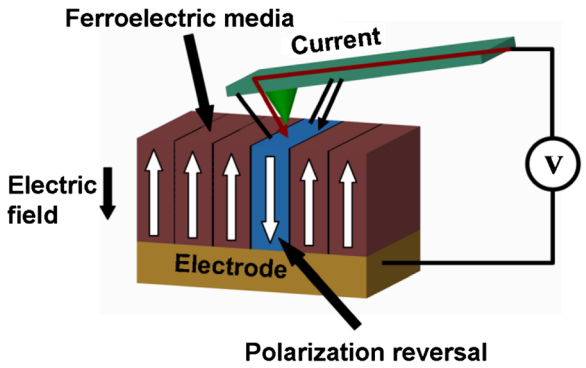

Fig. 9 Ferroelectric probe memory system

electronic charge in the crystal structure, whereas removing the electric field would drive dipole back to its original polarization state. Such a relationship can be simply interpreted by a hysteretic loop, as shown in Fig. 10. Therefore, these two distinct polarizations of dipole can be used to represent binary digits. During the recording process, a conductive probe where an external field is applied is brought in contact with the ferroelectric medium whose polarization can be switched according to the direction of the applied field. The readout process of ferroelectric probe memory adopts a very different mechanism from other probe storage memories, as its readout operation can only be conducted under "0" state. Consequently, no readout signal is detected for the case of reading "0" state. In contrast, to read "1" state, a current pulse is introduced to induce the polarization re-orientation, which is regarded as the readout signal. The readout process of ferroelectric probe memory apparently requires an erasing of the previously written data, which is known as "destructive readout" [58]. It should be kept in mind that ferroelectric materials, exemplified by lead zirconate titanate (PZT), has exhibited much higher energy density than the highest ever reported energy density for magnetic materials [59, 60]. Thanks to this, an unwanted thermal fluctuation effect induced by ambient thermal energy for ferroelectric materials would occur at a much higher density limit than magnetic materials. The density up to 3.6 Tb/in^2 on an atomically smooth PZT medium has been achieved [61]. The contrast in the positive and negative poling region can be significantly mitigated by either carefully controlling the deposition temperature or using the PZT films exposed to an ion beam using an electron cyclotron resonance (ECR) ion source with an argon and oxygen gas mixture [62]. The minimum single-digit domain with good stability in PZT film was recently reported to 4 nm in diameter, suggesting for a recording density of 40 $Tbit/in^2$ [63]. Another promising ferroelectric material in addition to PZT is $LiTaO_3$ that

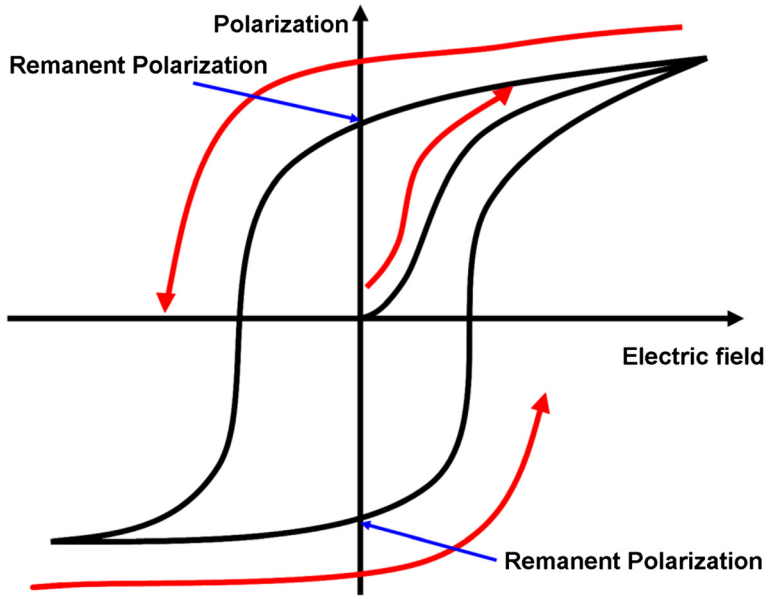

Fig. 10 Hysteretic loop of FeRAM

shows unique electro-optical properties as well as good mechanical and chemical stability [64–69]. The demonstration of accomplishing 10 Tbit/in^2 and 13 Tbit/in^2 using thin $LiTaO_3$ single-crystal films and a background field has been recently reported [70, 71]. For the latter case, data retention was measured by investigating the readback signals at elevated temperatures, and an activation energy of 0.8 eV at an attempt frequency of 200 kHz was found, sufficient for a data retention of 10 years [72].

Although the ferroelectric probe memory exhibits a capability of providing densities of multi-Tbit/in^2, its destructive readout mechanism requires data to be refreshed after readout and this would cumulate read/write cycles and eventually causes severe fatigue. In order to overcome the adverse effects of the destructive readout, several non-destructive readout methods have been recently proposed including piezoelectric force microscopy (PFM) readout [73–75] and scanning nonlinear dielectric microscopy (SNDM) readout [64, 76–78]. For PFM readout, a conductive probe where a small AC tip-sample voltage is applied is brought in contact with the sample, and the response of the probe related to the polarization state of ferroelectric domains is detected by PFM as a readout signal at a frequency below the cantilever resonance. It should be pointed out that the resulting electric field would possibly change the permittivity of the ferroelectric domain, thus resulting in an advent of second harmonics [73]. An alternative method to operate probe in non-contact mode is SNDM readout that possesses from a fact that the reversal of the ferroelectric polarization can slightly change the storage medium's capacitance due to the non-linearity in the permittivity tensor [79]. The variation on the capacitance would slightly change the resonance conditions that can be detected by monitoring the cantilever vibration if the cantilever is excited with a fixed AC voltage by means of a lock-in technique. Another method reported the direct piezoelectric effect to build up charge on the tip as a result of the tip-sample load force [78]. The resulting current is proportional to the load force, leading to a trade-off with endurance, as tip wear increases with the load force.

Phase-Change Probe Memory

Although the history of phase-change probe memory is fairly shorter than its compatriots, it has been considered as one of the most promising mass storage devices for the next generation due to its potential for ultra-high density, high data rate, long data retention, and low cost. Its advantageous characteristics arise from the combination of phase-change materials with nanoscale-conductive probe. Phase-change materials, mainly represented by chalcogenide alloy, are capable of exhibiting two distinct physical phases depending on the arrangement of the atomic structure [80], i.e., amorphous phase and crystalline phase. The atomic structure of amorphous phase presents a short range translational order, while for crystalline phase, the atoms are distributed in a repeating or periodic array over large atomic distances. Such a structural variation makes the electrical and optical properties of amorphous phase significantly different from the crystalline phase, as the phase-change materials in crystalline phase normally shows much

lower electrical resistivity and higher optical reflectivity than those of amorphous phase. Another intriguing feature of phase-change materials is that its two distinct phases can be switched between each other [81]. In order to generate crystalline phase, phase-change materials under amorphous phase needs to be heated above glass transition temperature but below the melting point, followed by a slow cooling to drive materials back to the energetically more favorable crystalline phase. To recover amorphous phase, phase-change materials in crystalline phase is required to be heated above melting temperature, subsequently followed by a fast quench to prevent the re-crystallization. Such a reversible transition is illustrated in Fig. 11. In addition to the thermal switching, a unique electronic switching phenomenon, known as "threshold switching", is also found on phase-change materials [82], which is depicted in Fig. 12. As can be seen from Fig. 12, a high-resistance state (OFF state) is initially presented in the phase-change materials along with the increase of the bias voltage, while a sudden "snap back" takes place when the bias voltage reaches a so-called threshold voltage. Under this circumstance, a sharp increase on the resulting current is monitored, leading to a low resistance state (ON state). Threshold switching is highly important for phase-change materials, as it allows for the phase transition at relatively low voltage. Otherwise, phase transition process can only be induced using very high voltage, thereby causing unnecessary energy consumption. Several theoretical models have been proposed to interpret the threshold switching from different scientific perspective. The threshold switching was first ascribed to the thermal breakdown effect in the amorphous film [83], whereas later, more evidence revealed that threshold switching was mainly dominated by electronic mechanism [84, 85]. According to this, two different electronic models based on trap-limited theory [86] and a balance between a strong Shockley Reed Hall (SRH) recombination through trap levels and a generation phenomenon [87] were, respectively, speculated to be the origin of the threshold switching. Differing from above models, a crystallization model owes the origin of threshold switching to the field induced nucleation of conductive cylindrical crystallites [88]. To date, the physical mechanism that can explicitly explain the threshold switching behavior still remains unclear.

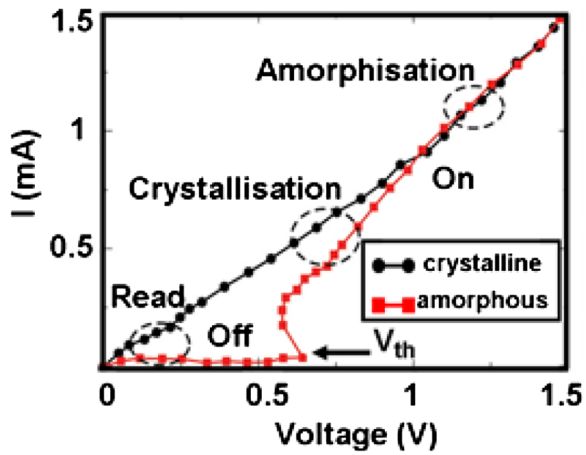

Fig. 12 Threshold switching phenomenon observed in phase-change materials. V_{th} is the threshold-switching voltage, and I represents the resulting current. Reprinted with permission from [82]

As phase-change materials in amorphous phase exhibit distinct electrical/optical properties from crystalline phase, it is viable for phase-change probe memory to utilize such properties difference to denote the binary digits "1" and "0". In terms of phase-change probe memory, during the recording process, a write current is injected to phase-change media through the conductive probe tip to either heat the media to crystalline temperature for crystallization, or to the melting temperature followed by a rapid cooling to generate amorphization. The readout process is achieved by detecting the difference on the sensing current between highly conductive crystalline state and highly resistive amorphous state. The operations of phase-change probe memory are schematically shown in Fig. 13. As the conductive probe is employed as the conductive path for writing current, the dimension of the resulting phase-transition region would strongly depend on the radius of tip apex. In other words, it is viable to achieve multi-

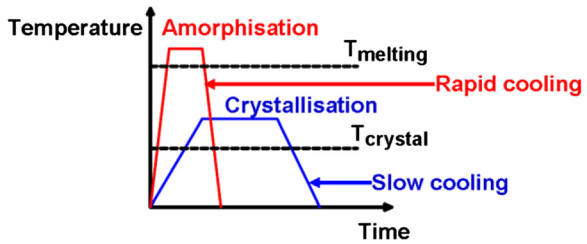

Fig. 11 Thermal switching of phase-change materials between amorphous and crystalline phases. T_m is the melting temperature and $T_{crystal}$ is the crystalline transition temperature

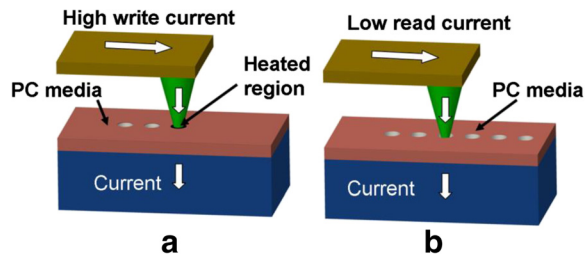

Fig. 13 Phase-change probe memory when operated in **a** write mode, and **b** read mode

Tbit/in^2 if the radius of the tip apex can be downscaled below around 20 nm [89]. In addition, the most commonly used storage medium in phase-change probe memory is $Ge_2Sb_2Te_5$, usually referred to GST, which has been extensively adopted by rewritable optical disc and phase-change random access memory due to its capability of offering fast transition speed, long data retention time, and great endurance [90–93]. Given that the nanoscale probe tip and the GST medium are two key components of the phase-change probe memory, it is natural to infer that phase change probe-memory is capable of inheriting the performance superiorities of the nanoscale probe and the GST media.

Depending on the adopted architecture of phase-change probe memory, a variety of resulting bit size from 80 to 20 nm has been reported [94–100]. By the time of writing, the maximum areal density of phase-change probe memory that can be achieved experimentally is up to 1 Tbit/in^2 [94] with corresponding power consumption of 100 PJ per bit [95], much lower than the thermo-mechanical probe memory. This is expected as phase-change probe memory requires the heating of bit volume only. Nevertheless, a new paradigm to induce the phase transition by a heated tip has recently been introduced [101], in which the AFM probe is heated to crystalline temperature either by a resistive heater or by a pulsed laser diode, and subsequently brought in contact with the GST to induce the phase transition. An areal density up to 3.3 Tb/in^2 was obtained with the desired write speed of 50 Mb/s for one probe when using a spinning disk to position the medium [101]. In addition, it is viable to achieve high density recording using a novel recording scenario that the probe moves a small distance over the media and thus gives rise to a recorded mark with "arbitrary" length by making use of the inter-symbol-interference (ISI) effect, also known as mark-length recording. The advantage of mark-length recording over the conventional mark-position recording arises from the independence of the resulting density on the size of the tip apex, allowing for an increase of user densities by at least 50 % and potentially 100 % with an implementation of relatively blunt tip [102]. A typical phase-change probe memory usually consists of a nanoscale conductive probe and a phase-change media stack that comprises a GST storage layer sandwiched by a capping layer and a under layer, which are all deposited on silicon (Si) or silicon dioxide (SiO_2) substrate. The role of capping layer is not only to protect GST layer from wear and oxidization, but also to build an effective electrically and thermally conductive path between probe tip and GST layer [103]. To satisfy the latter, the electrical conductivity of the capping layer needs to be relatively high in order to generate sufficient Joule heating inside the GST layer, while its thermal conductivity is required to be low to prevent heat from dissipating across the capping layer. However, a capping layer with high electrical conductivity is usually not desired as this would cause the presence of the short circuit during the readout process [104]. Compared with the capping layer, the under layer plays a less important role in determining the writing and readout performance of the phase-change probe memory, as it primarily acts as a bottom electrode. In this case, the electrical conductivity of the bottom layer is required to be much higher than capping layer so as to collect adequate write/readout current, while a relatively low thermal conductivity is preferable for the bottom layer to maintain sufficient Joule heat inside the storage layer [105, 106]. In addition, as both capping and bottom layers show thickness-dependent electrical/thermal conductivities [107, 108], their thicknesses also need to be carefully determined. Given the fact that threshold voltage is approximately equal to the product of layer thickness and threshold field, a thin GST is usually preferable so as to reduce the threshold voltage and thus the written power for a given low writing pulse. Therefore, an optimized design of the electrical probe memory device has been proposed by taking into account aforementioned factors as well as the underlying issues from practical fabrication process [109], as shown in Fig. 14. As can be seen from Fig. 14, this optimized phase-change media stack adopts a diamond-like-carbon (DLC) capping layer with thickness, electrical conductivity, and thermal conductivity of 2 nm, 100 $\Omega^{-1}m^{-1}$, 0.2 $Wm^{-1}K^{-1}$, and a titanium nitride (TiN) bottom layer with thickness, electrical conductivity, and thermal conductivity of 40 nm, 0.5×10^7 $\Omega^{-1}m^{-1}$, 12 $Wm^{-1}K^{-1}$, respectively. The thickness of GST layer is fixed to be 10 nm, which is the typical thickness for phase-change probe memory [89, 96]. The write and readout performances of the designed probe memory was assessed by a previously developed electro-thermal

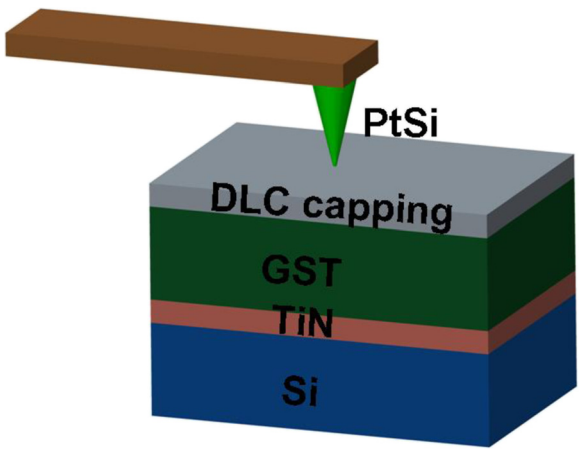

Fig. 14 An optimized phase-change probe memory architecture

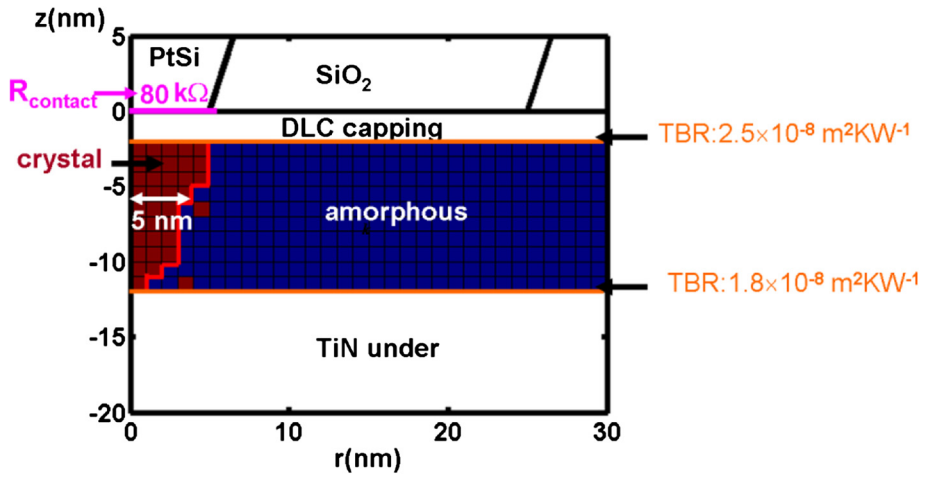

Fig. 15 The resulting crystalline bit from the designed optimal electrical probe memory. The written bit exhibits a radius of approximately 5 nm, corresponding to 10 Tbit/in^2

model that is, however, supplemented with several advanced modeling techniques including threshold switching, electrical contact resistance at PtSi/DLC interface, and thermal boundary resistance (TBR) at the interfaces of DLC/GST and GST/TiN [109]. The crystallization process in this model is determined by simultaneously solving the Laplace equation, classical heat transfer equation, and the nucleation-growth equation [6, 58, 103]. Solving the Laplace equation results in an electric field distribution inside the GST active layer, which is subsequently adopted as the Joule heating source for the classical heat transfer equation. Then, the temperature distribution inside the GST layer can be calculated by solving the heat transfer equation, whereby the temperature dependent crystal fraction of the GST layer can be obtained according to the nucleation-growth equation. Note that writing amorphous bit using electrical probe usually requires much higher temperature inside the capping layer than crystallization, and this may strongly harm the thermal stability of the capping layer. Because of this, the experimental writing of amorphous bits using electrical probe seems more difficult than writing crystalline bit, and was reported to be realized only by the stacks without capping layer [95, 110]. Therefore, in this paper, we are only taking into account the writing of crystalline bits. Figure 15 shows a production of a spherical shaped bit with a diameter of around 10 nm by a 6 V pulse of 100 ns, corresponding to the areal density of 10 Tb/inch^2 and the data rate of >Mb/s. Besides, the resultant writing power and writing energy are 0.016 mW and 1.6 pJ, respectively. This implies that the total writing energy required for using 100 and 1000 tips in parallel are 0.16 and 1.6 nJ, respectively, much lower than any other probe-based memories [11, 41, 67]. Most importantly, the crystalline bit shown in Fig. 15 is reported to be thermodynamically stable at the

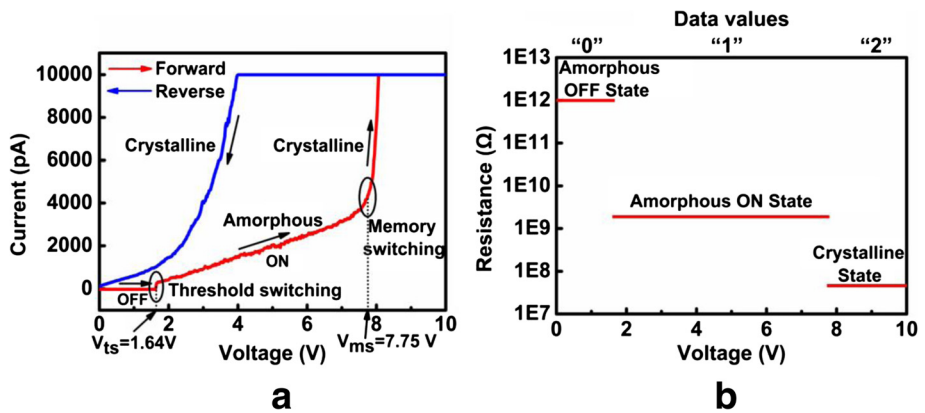

Fig. 16 **a** Current-voltage spectrum of amorphous GST thin film measured in the range of 0–10 V with C-AFM; **b** the corresponding resistance of the amorphous OFF state, amorphous ON state, and crystalline state. Reprinted with permission from [111]

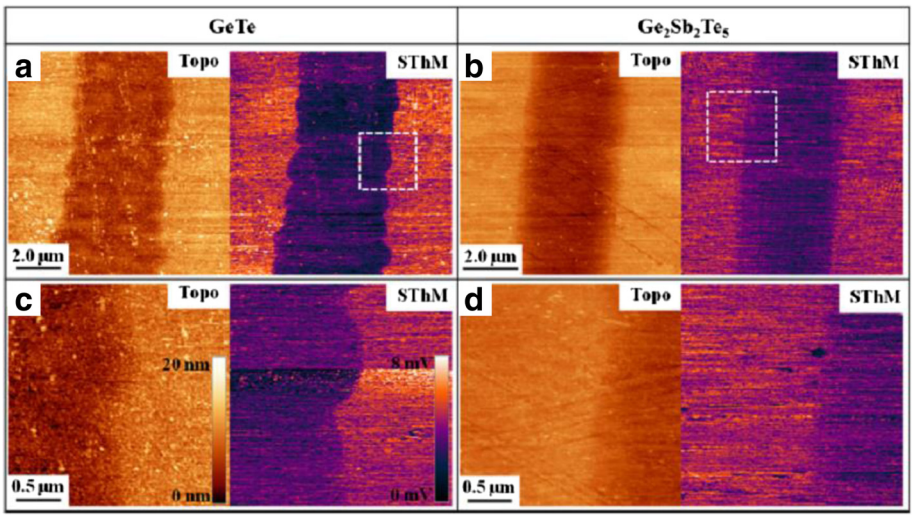

Fig. 17 **a** Topography (*left sub-panel*) and SthM (*right sub-panel*) images with 10 μm and **b** 8 μm scan sizes, revealing a crystalline line written into 200 nm GT and GST amorphous thin films by a focused laser beam. **c** The 2.5-μm images for GT and (**d**) GST taken from the spatial locations marked by the insets in **a** and **b**. Reprinted with permission from [112]

temperature below 550 °C, demonstrating its long retention time at archival temperature [89]. Meanwhile, the ability to achieve multi-level recording using phase-change probe memory was also demonstrated recently [111]. It was found that the resistance of the GST thin film can be toggled among three different states (high, intermediate, and low resistances) by carefully controlling the voltage between the conductive probe and the GST layer, as shown in Fig. 16. Therefore, three data values "0", "1", and "2" can be assigned to these three resistance states, respectively, allowing for multi-level operations in phase-change probe memory. In addition to the use of conductive AFM, scanning thermal microscopy (SThM) was recently reported to have the capability of measuring the thermal conductivities and thermal boundary resistances of GeTe (GT) and GST thin films [112, 113]. During the measurement, the SThM probe is repeatedly brought into and out of contact with material surface and the thermal properties of the probed materials can be determined by measuring the comparison of the heat flow from the SThM probe before and after the contact. According to such technique, it is possible to distinguish the amorphous phase from the crystalline phase by sensing the change in the thermal properties between amorphous and crystalline region, as revealed in Fig. 17. This finding also makes SThM as an alternative tool to provide bit write/read functions with spatial resolution down to the nanometer scale.

Conclusions

Today, the maximum achievable density resulting from conventional storage forms is currently limited below 1 Tb/in^2, and further density enhancement on these devices does not seem to be very optimistic provided that there are no innovative storage technologies emerging in the near future to break through their respective physical limits. Compared with the conventional storage devices, the practicality of using probe-based storage memories to achieve multi-Tbit/in^2 has been demonstrated on different probe storage devices. The characteristic comparison for different probe-based storage memories is shown in Table 1.

The advent of thermal-mechanical probe memory has pioneered a novel application of probe on data storage field and has been considered as the most mature probe technology in comparison to its juniors. However, the energy consumption caused by thermo-mechanical probe memory seems to be problematic as the entire tip

Table 1 Performance comparison of various probe memories [121]

	Phase-change	Magnetic	Thermomech	Ferroelectric
Density	3.3 Tb/in^2	60 Gb/in^2	4.0 Tb/in^2	4.0 Tb/in^2
Est. Max. density	≈10 Tb/in^2	≈100 Tb/in^2	≈10 Tb/in^2	>10 Tb/in^2
Read speed per probe	50 Mb s^{-1}	<10 b/s	40 kb s^{-1}	2 Mb s^{-1}
Write speed per probe	50 Mb s^{-1}	<10 b/s	1 Mb s^{-1}	50 kb s^{-1}
Travel per probe	2.5 m	0.5 m	750 m	5000 m

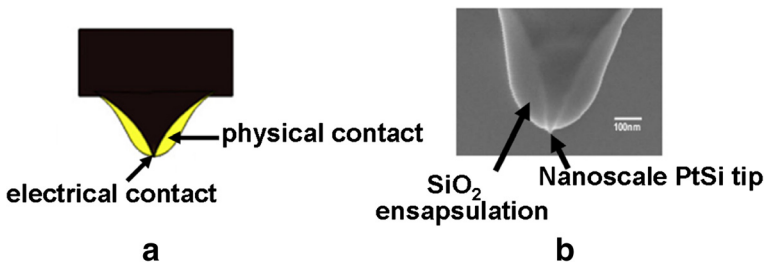

Fig. 18 **a** Schematic of the "encapsulated" tip concept, and **b** the experimentally fabricated encapsulated tip. Reprinted with permission from [117]

needs to be heated to perform write and readout process. This can be alleviated by a non-thermal writing mechanism that the AFM tip at room temperature is pressed into the polymer to generate the indentation [114]. This innovative writing strategy gives rise to a density up to 1 Tbit/in^2 or more with an exemption from heating the tip [114]. Due to the superparamagnetic limit, the maximum areal density obtained from magnetic probe memory in the laboratory level is limited to a few of Gbit/in^2, much lower than that of other probe storage memories. Moreover, the necessity to integrate a compliant cantilever with a sensitive force sensor for the readout of magnetic probe memory actually makes the array design more complicated. As a consequence, the practicality of magnetic probe memory is being strongly challenged, which may accelerate its demise in the future. Ferroelectric probe memory has recently received more attention than magnetic probe memory because of its higher density, faster readout speed, and more endurance cycles. In addition, several approaches aiming to reduce the tip wear have been recently examined. One possible way is to use a platinum iridium tip in the readout of ferroelectric media to increase the endurance of the tip [61]. It was found that no loss in either the read or the write resolution took place after a sliding distance of 5 km at 5 mm/s, resulting in an extremely low wear volume down to 5.6×10^3 nm^3. An alternative method to overwhelm tip wear is to implement a dielectric-sheathed carbon nanotube (CNT) probe with micrometer-long tips that can be immune to significant wear and ensure a high resolution for both write and readout processes [115]. Recently, a hard HfB_2 coated tip was reported to extend the tip's endurance beyond 8 km of sliding [116]. Benefiting from the merge of the nanoscale conductive tip and phase-change medium, the capability of phase-change probe memory to offer ultra-high density, fast write/readout speed, long retention time, and great endurance cycles has been demonstrated both experimentally and theoretically. A more attractive feature of phase-change probe memory than other probe storage devices arises from the fact that the conductive tip used in phase-change probe memory is only required to be electrically sharp rather than physically sharp. As a result, it is viable to fabricate an electrically sharp tip but with a large physical diameter, thereby mitigating tip tribology and wear issues without the sacrifice of the resulting density. Such an idea has indeed been experimentally demonstrated by the fabrication of a SiO_2-encapsulated silicon tip with platinum silicide (PtSi) at the tip apex [117, 118], as shown in Fig. 18. Forming PtSi at the tip apex can significantly improve the conduction and wear properties of the conductive tip, due to its ability to provide superior anti-wear characteristics and very high electrical conductivity. In addition, the use of the dielectric encapsulation (SiO_2) can increase the physical diameter of the tip and thus contribute to lower levels of wear due to the reduced pressure between tip and sample. Therefore, the integration of highly conductive PtSi tip apex with a non-conductive SiO_2 encapsulation assigns such an encapsulated tip a capability to present a very small electrical contact area with the media even if the tip itself is not physically very sharp, and consequently enables a high density writing and reading simultaneously with an extremely good anti-wear characteristic. Nevertheless, phase-change probe memory is severely limited by the difficulty of amorphizing crystalline regions of the storage medium [119, 120].

Acknowledgements
The authors acknowledge the financial support of the National Natural Science Foundation of China (grant No. 61201439).

Authors' contributions
LW performed the literature reviews of the thermo-mechanical probe memeory and the phase-change probe memory and drafted the manuscript; CHY performed the literature review of magnetic probe memory and edited the tables and figures; JW, SDG, and YXP performed the literature review of ferroelectric probe memory. All authors read and approved the final manuscript.

Competing interests
The authors declare that they have no competing interests.

Received: 23 June 2016 Accepted: 14 July 2016
Published online: 25 July 2016

References
1. Turner V (2014) Digital universe of opportunites. IDC Tech Report. 1
2. Wood R (2000) IEEE Trans Magn 36:36

3. Iwasaki S (2012) J Magn Magn Mater 324:244
4. Koide DC, Kajiyama T, Tokumaru H, Takano Y, Nabata Y, Ogata T, Miyazaki T, Ohishi K (2011) Jpn J Appl Phys 51:08JA04
5. Overton G (2012) Laser Focus World 48:39
6. Wang L, Gai S (2014) Contemp Phys 55:75
7. Lu CY (2012) J Nanosci Nanotechnol 12:7604
8. Lai SK (2012) J Nanosci Nanotechnol 12:7597
9. Binnig G, Quate CF (1986) Phys Rev Letts 56:930
10. Wright CD, Aziz MM, Shah P, Wang L (2011) Curr Appl Phys 11, e104
11. Vettiger P, Cross G, Despont M, Drechsler U, Durig U, Gotsmann B, Haberle W, Lantz MA, Rothuizen HE, Stutz R, Binnig GK (2002) IEEE Trans Nanotechnol 1:39
12. Binnig GK, Despont M, Drechsler U, Haberle W, Lutwyche M, Vettiger P, Mamin HJ, Chui BW, Kenny TW (1999) Appl Phys Lett 74:1329
13. Pozidis H, Haberle W, Wiesmann D, Drechsler U, Despont M, Albrecht TR, Eleftheriou E (2004) IEEE Trans Magn 40:2531
14. Vettiger P, Despont M, Drechsler U, Durig U, Haberle W, Lutwyche MI, Rothuizen HE, Stutz R, Widmer R, Binnig GK (2000) IBM J Res & Dev 44:323
15. Cannara RJ, Gotsmann B, Knoll A, Durig U (2008) Nanotechnology 19:395305
16. King WP, Santiago JG, Kenny TW, Goodson KE (1999) Proc ASME MEMS 1:583
17. Wiesmann D, Rawlings C, Vecchione R, Porro F, Gotsmann B, Knoll A, Pires D, Duerig U (2009) Nano Letts 9:3171
18. Gotsmann B, Duerig U, Frommer J, Hawker CJ (2006) Adv Funct Mater 16:1499
19. Pires D, Gotsmann B, Porro F, Wiesmann D, Durig U, Knoll A (2009) Langmuir 25:5141
20. Knoll A, Wiesmann D, Pires D, Gotsmann B, Durig U (2010) J Nanosci Nanotechnol 10:4538
21. Gotsmann B, Knoll AW, Pratt R, Frommer J, Hedrick JL, Durig U (2010) Adv Funct Mater 20:1276
22. H. J. M, J. S. Trethewey, A. D. Johnson, W. J. Drugan, and W. C. Crone, Adv. Maters. 17, 1123(2005).
23. Shaw GA, Trethewey JS, Johnson AD, Drugan WJ, Crone WC (2005) Adv Maters 17:1123
24. Bhaskaran H, Gotsmann B, Sebastian A, Drechsler U, Lantz MA, Despont M, Jaroenapibal P, Carpick RW, Chen Y, Sridharan K (2010) Nat Nanotechnol 5:181
25. Lantz MA, Gotsmann N, Jaroenapibal P, Jacobs TDB, O'Connor SD, Sridharan K, Carpick RW (2012) Adv Funct Mater 22:1639
26. Sahoo DR, Haberle W, Bachtold P, Sebastian A, Pozidis H, Eleftheriou E (2008) 2008 American Control Conference. ACC, Seattle, pp 2034–2039
27. Knoll A, Rothuizen H, Gotsmann B, Duerig U (2010) Nanotechnol 21:185701
28. Lantz MA, Wiesmann D, Gotsmann B (2009) Nat Nanotechnol 4:586
29. Shalaby M, Vicario C, Hauri CP (2016) New J Phys 18:013019
30. Mironov VL, Ermolaeva OL (2009) J Surf Invest 3:840
31. Mironov VL, Gribkov BA, Vdovichev SN, Gusev SA, Fraerman AA, Ermolaeva OL, Shubin AB, Alexeef AM, Zhdan PA, Binns C (2009) J Appl Phys 106:053911
32. Onoue T, Siekamn M, Abelmann L, Lodder JC (2004) J Magn Magn Mater 272:2317
33. Ohkubo T, Kishigami J, Yanagisawa K, Kaneko R (1991) IEEE Trans Magn 27: 5286
34. Ohkubo T, Kishigami J, Yanagisawa K, Kaneko R (1993) NTT R&D 42:545
35. Ohkubo T, Maeda Y, Koshimoto Y (1995) IEICE Trans On Electron E78-C:1523
36. Manalis S, Babcock K, Massie J, Elings V, Dugas M (1995) Appl Phys Lett 66:2585
37. El-Sayed RT, Carley LR (2004) IEEE Trans Magn 40:2326
38. El-Sayed RT, Carley LR (2003) IEEE Trans Magn 39:3566
39. Zhang L, Bain JA, Zhu J-G, Abelmann L, Onoue T (2007) Physica B 387:328
40. Zhong ZY, Zhang L, Zhang H-W (2008) Curr Appl Phys 8:57
41. Zhang L, Bain JA, Zhu J-G, Abelmann L, Onoue T (2006) J Magn Magn Mater 305:16
42. Zhang L, Bain JA, Zhu J-G (2002) IEEE Trans Magn 38:1895
43. Zhang L, Bain JA, Zhu J-G, Abelmann L, Onoue T (2004) IEEE Trans Magn 40:2549
44. Watanuki O, Sonobe Y, Tsuji S, Sai F (1991) IEEE Trans Magn 27:5289
45. Hosaka S, Koyanagi H, Kikukawa A, Miyamoto M, Imura R, Ushiyama J (1995) J of Vac Sci &Technol B 13:1307
46. Nakamura J, Miyamoto M, Hosaka S, Koyanagi H (1995) J Appl Phys 77:779
47. Zhong ZY, Zhang L, Zhang HW (2007) EPJ Appl Phys 38:259
48. Onoue T, Siekman H, Abelmann L, Lodder JC (2008) J Appl Phys D 41: 155008
49. Algre E, Gaudin G, Bsiesy A, Nozieres JP (2005) IEEE Trans Magn 41:2857
50. Watson CS, Hollar C, Anderson K, Knowlton WB, Mullerner P (2013) Adv Funct Mater 23:3995
51. E. Sarajlic, R. Vermeer, M. Y. Delalande, M. H. Siekman, R. Huijink, H. Fujita, and L. Abelmann. in: Oric, 23rd Ubt, Conf. on Micro Electro Mechanical Systems (MEMS 2006), Hong Kong, 2010, 328(2010).
52. Petit D, Atkinson D, Johnston S, Wood D, Cowburn RP (2004) IEE Proc: Science. Measurement and Technology 151:127
53. Oral A, Bending SJ, Henini M (1996) Appl Phys Lett 69:1324
54. Gregusova D, Martaus J, Fedor J, Kudela R, Kostic I, Cambel V (2009) Ultramicroscopy 109:1080
55. Hatakeyama K, Vermeer R, Siekman MH, Sarajlic E, Tas NR, Abelmann L (2014) In: INTERMAG 2014, Dresden. pp. 1741–1742. IEEE
56. Takezaki T, Yagisawa D, Sueoka K (2006) Jpn J Appl Phys 45:2251
57. Precner M, Fedor J, Soltys J, Cambel V (2015) Nanotechnol 26:055304
58. Wang L, Yang CH, Wen J (2015) Electron Mater Lett 11:505
59. Pertsev NA, Contreras JR, Kukhar VG, Hermanns B, Kohlstedt H, Waser R (2003) Appl Phys Lett 83:3356
60. Zybill CE, Li B, Koch F, Graf T (2000) Phys Status Solidi A 177:303
61. Tayebi N, Zhang Y, Chen RJ, Tran Q, Chen R, Nishi Y, Ma Q, Rao V (2010) ACS Nano 4:5713
62. Hiranaga Y, Cho Y (2014) Jpn J Appl Phys 53:09PA05
63. Tayebi N, Narui Y, Franklin N, Collier CP, Giapis KP, Nishi Y, Zhang Y (2010) Appl Phys Lett 96:023103
64. Cho Y, Fujimoto K, Hiranaga Y, Wagatsuma Y, Onoe A, Terabe K, Kitamura K (2002) Appl Phys Lett 81:4401
65. Cho Y, Hashimoto S, Odagawa N, Tanaka K, Hiranaga Y (2005) Appl Phys Lett 87:232907
66. Hiranaga Y, Fujimoto K, Cho Y, Wagatsuma Y, Onoe A, Terabe K, Kitamura K (2002) Integr Ferroelectr 49:203
67. Cho Y, Fujimoto K, Hiranaga Y, Wagatsuma Y, Onoe A, Terabe K, Kitamura K (2003) Nanotechnol 14:637
68. Hiranaga Y, Cho Y, Fujimoto K, Wagatsuma Y, Onoe A (2003) Jpn J Appl Phys 42:6050
69. Cho Y, Hiranaga Y, Fujimoto K, Wagatsuma Y, Onoe A (2004) Integr Ferroelectr 61:77
70. Cho Y, Fujimoto K, Hiranaga Y, Wagatsuma Y, Onoe A, Terabe K, Kitamura K (2003) Ferroelectrics 292:51
71. Hiranaga Y, Uda T, Kurihashi Y, Tanaka K, Cho Y (2007) IEEE Trans Ultrason Ferr Freq Control 54:2523
72. Tanaka K, Hiranaga Y, Cho Y (2008) Record of electrical and commun. Eng Conversazione Tohoku University 76:384
73. Franke K, Besold J, Haessler W, Seegebarth C (1994) Surf Sci 302:L283
74. Hidaka T, Maruyama T, Saitoh M, Mikoshiba N, Shimizu M, Shiosaki T, Wills LA, Hiskes R, Dicarolis SA, Amano J (1996) Appl Phys Lett 68:2358
75. Kalinin SV, Jesse S, Rodriquez BJ, Shin J, Baddorf AP, Lee HN, Borisevich A, Pennycook SJ (2006) Nanotechnol 17:3400
76. Saurenbach F, Terris BD (1990) Appl Phys Lett 56:1703
77. Saurenbach F, Terris BD (1992) IEEE Trans Ind Appl 28:256
78. Kim BM, Adams DE, Tran Q, Ma Q, Rao V (2009) Appl Phys Lett 94:063105
79. Tanaka K, Kurihashi Y, Uda T, Daimon Y, Odagawa N, Hirose R, Hiranaga Y, Cho Y (2008) Jpn J Appl Phys 47:3311
80. Wuttig M, Yamada N (2007) Nature 6:824
81. Matheswaran P, Sathyamoorthy R, Asokan K (2012) Electron Mater Lett 8:417
82. Welnic W, Wuttig M (2008) Materials Today 11:20
83. Adler D, Henisch HK, Mott N (1978) Rev Mod Phys 50:209
84. Adler D, Shur MS, Silver M, Ovshinsky SR (1980) J Appl Phys 51:3289
85. Adler D, Shur MS, Silver M, Ovshinsky SR (1984) J Appl Phys 56:579
86. Ielmini D, Zhang YG (2007) J Appl Phys 102:054517
87. Redaelli A, Pirovano A, Benvenuti A, Lacaita AL (2008) J Appl Phys 103: 111101
88. Karpov VG, Kryukov YA, Savransky SD, Karpov IV (2007) Appl Phys Lett 90: 123504
89. Wright CD, Marilyn M, Mustafa MM (2006) IEEE Trans Nanotechnol 5:50
90. Yamada N, Ohno E, Nishiuchi K, Akahira N, Takao M (1991) Jpn J Appl Phys 69:2849
91. Kolobov AV, Fons P, Tominaga J, Uruga T (2006) J Non-Cryst Solids 352:1612
92. Wong H-SP, Raoux S, Kim SB, Liang JL, Reifenberg JP, Rajendran B, Asheghi M, Goodson KE (2010) Proc IEEE 98:2201
93. Raoux S, Welnic W, Ielmni D (2010) Chem Rev 10:240

94. Gidon S, Lemonnier O, Rolland B, Bichet O, Dressler C, Samson Y (2004) Appl Phys Lett 85:6392
95. Satoh H, Sugawara K, Tanaka K (2006) J Appl Phys 99:024306
96. Bhaskaran H, Sebastian A, Pauza A, Pozidis H, Despont M (2009) Rev Sci Instrum 80:083701
97. Wang L, David CD, Shah P, Aziz MM, Sebastian A, Pozidis H, Pauza A (2011) Jpn J Appl Phys 50:09MD04
98. Wang L, Wright CD, Aziz MM, Shah P, Yang CH, Yang GW (2013) Mater Lett 112:51
99. Wang L, Wright CD, Aziz MM, Yang CH, Yang GW (2016) Electron Mater Lett 10:1045
100. Wang L, Gong SD, Wen J, Yang CH (2016) J Nanomater 2016:1
101. Hamann HF, O'Boyle M, Martin YC, Rooks M, Wickramasinghe HK (2006) Nat Mater 5:383
102. Wright CD, Shah P, Wang L, Aziz MM, Sebastian A, Pozidis H (2010) Appl Phys Lett 97:173104
103. Wang L, Yang CH, Wen J, Gai S, Peng YX (2015) J Mater Sci Mater Electron 26:4618
104. Wang L, Wright CD, Aziz MM, Yang CH, Yang GW (2014) Jpn J Appl Phys 53: 028002
105. Wang L, Wright CD, Aziz MM, Ying J, Yang GW (2013) EPL 104:56007
106. Wang L, Wen J, Yang CH, Shan G, Miao XS (2015) Nanosci Nanotechnol Lett 7:870
107. Balandin AA, Shamsa ML, Liu WL, Casiraghi C, Ferrari AC (2008) Appl Phys Lett 93:043115
108. Shamsa M, Liu WL, Balandin AA, Casiraghi C, Milne WI, Ferrari AC (2006) Appl Phys Lett 89:161921
109. Wang L, Wen J, Yang CH, Gai S, Peng YX (2015) Nano 10:1550118
110. Wright CD, Wang L, Shah P, Aziz MM, Varesi E, Bez R, Moroni M, Cazzaniga F (2011) IEEE Trans Nanotechnol 10:900
111. Yang F, Xu L, Chen J, Xu J, Yu Y, Ma ZY, Chen K-J (2016) Nanotechnology 27:035706
112. Bo JL, Timofeeva M, Tovee PD, Robinson BJ, Huey BD, Kolosov OV (2014) J Appl Phys 116:134904
113. Velea A, Borca CN, Socol G, Galca AC, Grolimund D, Popescu M, van Bokhoven JA (2014) J Appl Phys 116:234306
114. Jo A, Joo W, Jin WH, Nam H, Kim JK (2009) Probe-based data storage. Nature Nanotechnol 4:727.
115. Tayebi N, Narui A, Chen RJ, Collier CP, Giapis KP, Zhang Y (2008) Appl Phys Lett 93:103112
116. Tayebi N, Yanguas-Gil A, Kumar N, Zhang Y, Abelson JR, Nishi Y, Ma Q, Rao VR (2012) Appl Phys Lett 101:091909
117. Bhaskaran H, Sebastian A, Drechsler U, Despont M (2009) Nanotechnol 20: 105701
118. Bhaskaran H, Sebastian A, Despont M (2009) IEEE Trans Nanotechnol 8:128
119. Wang L, Yang CH, Wen J, Peng YX (2015) Current Nanoscience 11:676.
120. Tanaka K (2007) J Non-Crystals Solids 353:1899
121. W. W. Koelmans, J. B. C. Engelen, and L. Abelmann. arXiv. 1(2015).